THE JOURNAL OF PHYSICAL CHEMISTRY Letters

pubs.acs.org/JPCL Letter

Direct Visualization of Hydrogen-Transfer Intermediate States by Scanning Tunneling Microscopy

Rongting Wu,[¶] De-Liang Bao,[¶] Linghao Yan, Yeliang Wang, Junhai Ren, Yan-Fang Zhang, Qing Huan,* Yu-Yang Zhang, Shixuan Du,* Sokrates T. Pantelides, and Hong-Jun Gao*

Cite This: *J. Phys. Chem. Lett.* 2020, 11, 1536−1541 Read Online

ACCESS | Metrics & More | Article Recommendations | Supporting Information

ABSTRACT: Hydrogen atoms bonded within molecular cavities often undergo tunneling or thermal-transfer processes that play major roles in diverse physical phenomena. Such transfers may or may not entail intermediate states. The existence of such fleeting states is typically determined by indirect means, while their direct visualization has not been achieved, largely because their concentrations under equilibrium conditions are negligible. Here we use density-functional-theory calculations and scanning-tunneling-microscopy (STM) image simulations to predict that, under specially designed nonequilibrium conditions of voltage-enhanced high transfer rates, the *cis*-intermediate of the two-hydrogen transfer process in metal-free naphthalocyanine molecules adsorbed on Ag(111) surfaces would be visualizable in a composite image of double-C morphology. As guided by the theoretical predictions, at adjusted scanning temperature and bias, STM experiments achieve a direct visualization of the *cis*-intermediate. This work demonstrates a practical way to directly visualize elusive intermediates, which enhances understanding of the quantum dynamics of hydrogen atoms.

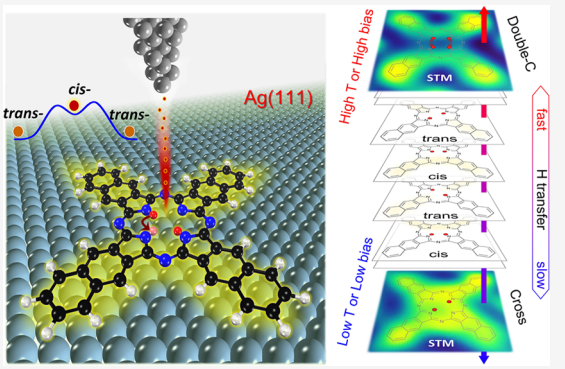

Hydrogen transfer, whether by tunneling or by thermal activation, is one of the most fundamental atomic-scale processes in physics, chemistry, and biology and plays a major role in important phenomena such as DNA replication,[1] enzyme-catalyzed reactions,[2,3] and photosynthesis.[4] On-surface molecules and molecular clusters have been designed as prototypes for the investigation of the hydrogen-transfer process.[5−8] Multiple configurations of more than one hydrogen atom are known as tautomers and the interconversion between configurations is known as tautomerization. In some cases, the hydrogen atoms transfer to equivalent positions in a concerted way with no intermediate state. The distinct initial and final tautomers can be detected by measuring distinct STM currents from them, as in the case of a four-water-molecule cluster.[9] In other cases, the hydrogen atoms transfer via a distinct intermediate state. An example is the porphyrin molecule,[10] in the central cavity of which there are two hydrogens and four positions at the corners of a square. The two hydrogens occupy positions across from each other (*trans*-configuration) and transfer to the equivalent configuration defined by the other two positions.[7,10] Transfer can in principle be concerted, i.e., the two hydrogens tunnel simultaneously to their new positions or be via an intermediate state in which the two hydrogens occupy adjacent positions (*cis*-configuration). The existence of such an intermediate state has been demonstrated in porphyrin by nuclear magnetic resonance (NMR) spectroscopy,[11−13] fluorescence spectra,[13,14] and UV/visible[15] or infrared[16] photoexcitation. In a lower-symmetry molecule (porphycene) or a complex molecule containing porphyrin, the *cis*-configuration was recently found to be the ground state while the *trans*-configuration is the intermediate.[17−20] In cases when there are intermediate states, only the initial and final states have been visualized in STM images.[7,18−21] It has not been possible so far to directly visualize the intermediate states in STM images, largely because the equilibrium concentrations of these higher-energy states are negligible.

It has been found that intramolecular two-hydrogen-transfer processes in macrocyclic-aromatic molecules (porphycene,[21] porphyrin,[22] and naphthalocyanine[7]) have intermediate states and show great tunability by STM. With imaging at low bias voltage, the transfer rate is essentially purely thermal and the different configurations exist at equilibrium concentrations. When the bias voltage or tunneling current between the tip and the substrate is increased, the two-hydrogen-transfer rate increases in a roughly exponential[7] or linear[22] fashion, respectively. Such tip-assisted transfer can be attributed to the excitation of specific molecular vibrations.[20] Moreover, the

Received: January 6, 2020
Accepted: February 3, 2020
Published: February 3, 2020

https://dx.doi.org/10.1021/acs.jpclett.0c00046
J. Phys. Chem. Lett. 2020, 11, 1536−1541

hydrogen-transfer rate can be tuned up and down in a controlled fashion by a copper adatom placed close to the molecule with atomic precision.[18] An external force induced by the tip has been demonstrated to reduce the effective activation barriers and plays a catalyst role in the transfer process.[19] All these successes bring STM to the technical edge for the observation of the fleeting metastable intermediate states of hydrogen transfer in tautomerization processes.

In this paper, we report evidence of directly visualizing the *cis*-intermediates during the stepwise hydrogen-transfer process in the inner cavity of metal-free naphthalocyanine (NPc) molecules by combining experimental STM images, simulated STM images, and density-functional-theory (DFT) calculations. A key initial calculation reveals that the *cis*-configuration is a metastable state and its concentration is negligible at practical temperatures under equilibrium conditions. We, therefore, seek to image a superposition of configurations under nonequilibrium conditions and rely on the following three enablers. The first enabler is the fact that scanning at room temperature (RT) and high bias voltage (HV) substantially increases the hydrogen-transfer rate. Thus, during the scanning period, which is very long compared with the transfer period, all *trans*- and *cis*-configurations contribute appreciably to the resulting image. The second enabler is a result of DFT calculations: considering the effect of the substrate, we find that the energy barriers of two specific transfer paths are lower; i.e., a select number of configurations dominate the image. Finally, the third enabler is also a result of DFT calculations: we demonstrate that, at high bias voltage, the *cis*-configuration contributes a unique C-shaped component to the composite image. Given the above, we derive simulated STM images at RT as follows. At low scanning bias, the STM images a superposition of the configurations that exist at high concentrations under equilibrium conditions, namely, the two *trans*-configurations, resulting in the well-known cross-like STM-image morphology. Under nonequilibrium conditions, however, at sufficiently high scanning bias and room temperature, the imaging time is much longer than the transfer time, enhancing the presence of the intermediate configuration. The *cis*-intermediate configuration is then predicted to manifest itself in a symmetric-double-C morphology arising from the superposition of two *trans*-configurations and two opposite metastable *cis*-configurations. For the experiments, a monolayer of NPc molecules was fabricated on a Ag(111) surface by self-assembly. At low bias voltages between 0 and −1.8 V, the usual cross-like images are observed[23] at room temperature. When the scanning bias voltage is increased to −2.5 V, the STM morphology of the NPc molecule changes from the cross-like shape to a symmetric-double-C shape, confirming the presence of the *cis*-configurations. At 100 K, both theory and experiments find an image with asymmetric double-C morphology, confirming the mechanism that underlying the imaging process. Overall, the present results demonstrate a scheme by which intermediate states in two-hydrogen-transfer processes can be visualized.

H transfer in Freestanding NPc Molecule. The NPc molecule comprises a phthalocyanine (Pc) skeleton with an additional benzene ring attached to each of the four arms that extend from four pentagonal "lobes" (Figure 1a). It has a planar geometry with a van der Waals diameter of approximately 2 nm. In its ground-state configuration, the two hydrogen atoms in the inner cavity bond to two opposite pyrrolic nitrogen

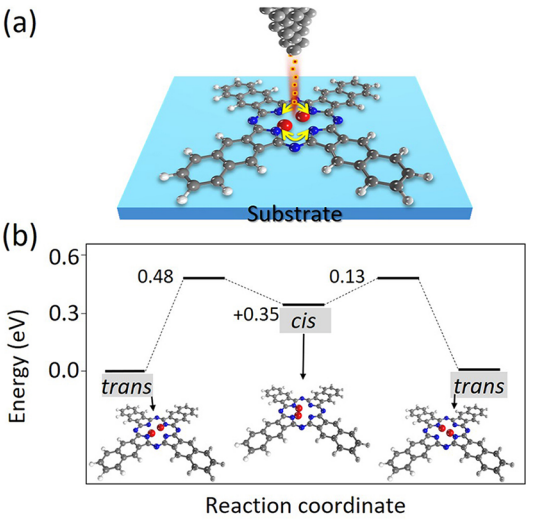

Figure 1. Stepwise hydrogen-transfer process in NPc molecules. (a) Schematic diagram of the experimental STM procedure that was employed to probe the two-hydrogen-transfer process in the inner cavity of NPc molecules on Ag(111) surface. The yellow arrows denote the hydrogen-transfer path. (b) DFT-calculated energy path for the hydrogen-transfer process and the atomic models of the NPc molecule in *trans*-configuration (left), *cis*-configuration (middle), and *trans*-configuration (right), respectively.

atoms forming a *trans*-configuration. We shall refer to lobes with a bonded hydrogen as "H-lobes" and to lobes without a hydrogen as "no-H-lobes".

It is instructive to first examine the two-hydrogen-transfer process in a free NPc molecule, as illustrated in Figure 1b. Switching the two hydrogen atoms to the other pair of opposite pyrrole nitrogen atoms produces an equivalent but distinct *trans*-configuration. During the stepwise-transfer path between the two *trans*-configurations, the system goes through a *cis*-configuration state,[10,11] whose energy is higher by 0.35 eV. All energy barriers are considerably smaller than 1 eV, which suggests that transfers occur at substantial rates at RT.[10,11,14]

The relative energies of the *trans*- and intermediate *cis*-configurations for a stepwise two-hydrogen-transfer in the free NPc molecule together with the pertinent energy barriers are shown in Figure 1b. Since the energy of the metastable *cis*-configuration is 0.35 eV higher than the energy of the *trans*-configurations, its equilibrium concentration at RT is smaller than the equilibrium concentration of the *trans*-configurations by 7 orders of magnitude. This difference in energies persists in on-surface molecules (see below), whereby it is impossible to image the *cis*-configuration under equilibrium conditions. There is another option, however. Under conditions of high transfer rate, when the transfer period is significantly smaller than the time it takes to collect an image, on average, the *trans*- and *cis*-configurations should be present for comparable times. The details are then controlled by the energy barriers along the transfer paths. We, therefore, turn our attention to the energy barriers.

H Transfer in On-Surface NPc Molecules. In the freestanding case, the four *cis*-configurations that can be labeled by the placement of the two adjacent hydrogens, i.e. top, down, left, and right, respectively, are equivalent. In the on-surface case, taking the center of the molecule's square inner cavity as a reference, the cavity can be located at top, bridge, fcc, or hcp sites on a Ag(111) surface (Supplementary Figure 4). In all

https://dx.doi.org/10.1021/acs.jpclett.0c00046
J. Phys. Chem. Lett. 2020, 11, 1536−1541

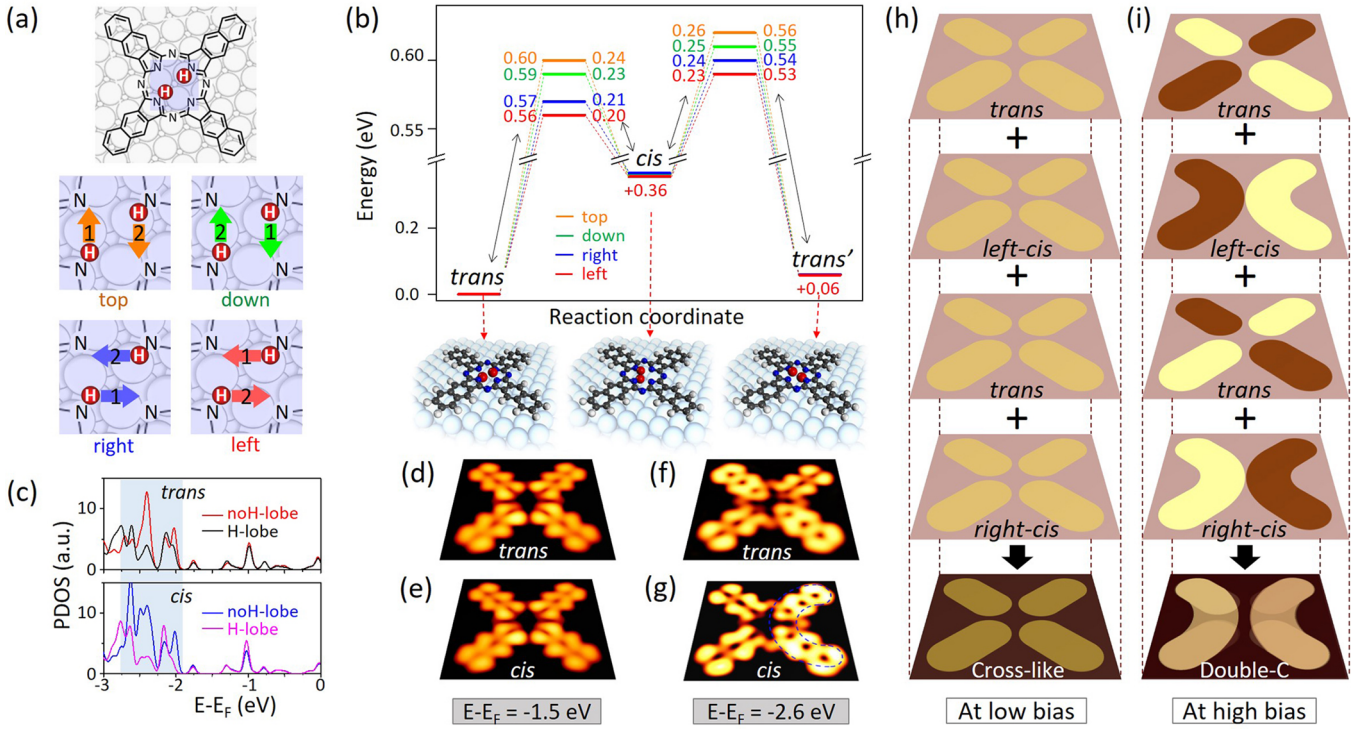

Figure 2. Stepwise two-hydrogen-transfer process in a NPc molecule adsorbed at fcc site on Ag(111) and STM simulations. (a) Schematic diagrams of the four stepwise-transfer paths on a Ag(111) surface. The arrows and numbers represent the transfer directions and sequences of the two hydrogens, respectively. (b) DFT-calculated energy profiles for the four transfer paths and the atomic models of the initial *trans*-, intermediate left *cis*-, and final *trans*′-configurations. (c) PDOS on the no-H-lobe and the H-lobe for the *trans*- and *cis*-configurations, respectively. (d)−(g) Simulated STM images of the *trans*- and *cis*-configurations at low and high bias voltages, respectively. (h)−(i) Schematic diagrams of cross-like morphology and double-C-shaped morphology produced by the superposition of both *trans*-configurations and two energy-favored *cis*-configurations at low (h) and high (i) bias voltage, respectively.

cases, the four H-transfer processes are no longer equivalent. We have examined representative configurations at each site and, though the presence of the substrate reduces the symmetry of the molecule somewhat differently, the energy barriers for the four possible transfer paths split into the same two lower-energy-barrier paths and two higher-energy-barrier paths. Here we discuss the case of fcc adsorption site, at which the system's energy is lowest. Similar results for other representative adsorption sites can be found in Supplementary Figure 5. This feature will prove crucial to our ability to image the intermediate *cis*-configuration.

The molecule's configurations and energy barriers for H transfers are calculated at T = 0 K in the absence of bias. We shall use these results to analyze the hydrogen-transfer processes at high bias and at finite temperatures (300 and 100 K), as we do not anticipate significant configuration changes because the molecules are bonded to the substrate by weak van der Waals interactions and remain flat as in their free-standing state. Indeed, the STM images that will be described below show flat molecules at both temperatures of interest and both low and high bias. In Figure 2a, starting with a *trans*-configuration, we designate the pathways that contain each of the four *cis*-configurations (in each case, the two steps in the two-step-transfer process are designated as 1 and 2). The energy profiles of the four possible transfer paths and the atomic models of the on-surface initial *trans*-configuration, left *cis*-configuration, and final *trans*′-configuration for the lowest-energy path are shown in Figure 2b. It is notable that the four paths are divided into two groups according to the barriers. The rate-determining-step barriers of the left and right paths are lower than those of the top and down ones, indicating that, at moderate temperatures, the transfer probability via the left and right paths is larger than via the top and down paths. The same is true for the reverse processes. In the Supporting Information, we demonstrate that thermal transfer is dominant over tunneling at RT. Based on the calculated energy barriers, the percent contributions to the total forward and reverse transfer rates for molecules adsorbed at fcc, bridge, and top sites on the Ag(111) surface are such that the left and right paths, featuring left and right *cis*-configurations, are the main contributors to the composite morphology (see Supplementary Table 1 and Figure 2). This result is very important for the prediction of the STM images at different temperatures.

Electronic Distribution at H- and No-H-Lobes in NPc. As STM is sensitive to the electron density in the range of energies spanned by the bias voltage,[24,25] we calculated the projected density of states (PDOS) on the H- and no-H-lobes of both the *trans*- and *cis*-configurations in the lowest-energy-barrier path (Figure 2c). We note immediately that for low bias voltages, which sample electrons in the energy range from the Fermi energy (0 eV) to about −2.0 eV, the PDOS on the H- and no-H-lobes are essentially the same for *trans*- and *cis*-configurations. Simulated STM images for both a *trans*- and a *cis*-configuration at −1.5 V (low bias) show cross-like morphologies (no difference between the H- and no-H-lobes) (Figure 2d,e, respectively). Thus, the theory so far predicts that STM images taken at low bias at RT would have the cross-like morphology.

At higher bias voltages, however, sampling the energy range deeper than −2.0 eV, the PDOS on the no-H-lobe is larger

https://dx.doi.org/10.1021/acs.jpclett.0c00046
J. Phys. Chem. Lett. 2020, 11, 1536−1541

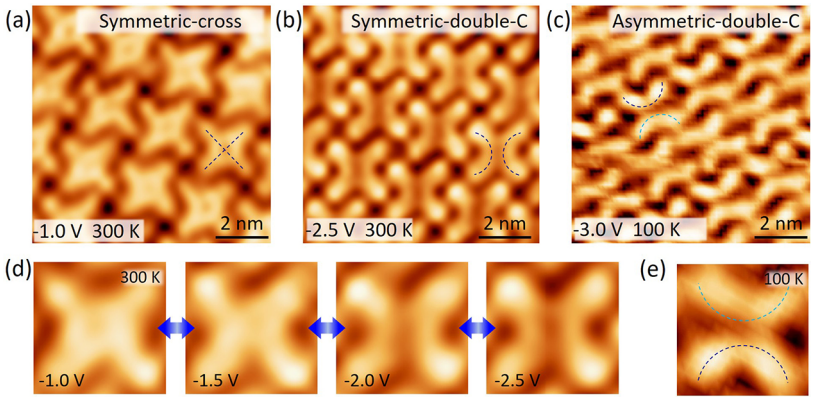

Figure 3. Different STM morphologies of NPc molecules on the Ag(111) surface. (a) Typical cross-like morphology of NPc molecules in the self-assembly monolayer on Ag(111) (scanning recipe: −1.0 V, 0.1 nA, RT). (b) Symmetric-double-C morphology of NPc molecules in the same area in (a) (scanning recipe: −2.5 V, 0.1 nA, RT). (c) Asymmetric-double-C morphology of monolayer NPc on Ag(111) (scanning recipe: −3.0 V, 0.1 nA, 100 K). The dark- and light-blue dashed curves highlight the asymmetric-double-C morphology. Here the lowest-barrier path dominates. (d) Continuous and reversible transition between cross-like and symmetric-double-C morphologies by regulating the scanning bias. (e) At 100 K and high bias, a zoom-in asymmetric double-C image (scanning recipe: −2.8 V, 0.1 nA, 100 K).

than that on the H-lobe for both the *trans*- and *cis*-configurations (blue shading in Figure 2c). In corresponding STM simulations at energy −2.6 V (high bias), one can see that a single *trans*-configuration appears as a somewhat asymmetric cross (Figure 2f), while the *cis*-configuration exhibits a "single-C" shaped morphology (Figure 2g). Therefore, the "asymmetric-cross" and "single-C" shaped morphologies can be regarded as the high-bias-voltage "fingerprints" of a single *trans*-configuration and a single *cis*-configuration, respectively.

Double-C-Shaped "Fingerprints" of the Cis-Configuration State at High Bias Voltage. As noted already, since the scanning time of a typical STM image is several minutes, the observed image can be regarded as a statistical superposition of all possibilities of the in situ tautomerization reactions. Since each transfer process always entails both *trans*-configurations and a *cis*-configuration, assuming that the high-bias enhancement of the H-transfer rate also favor the lower-energy pair of energy barriers, the predicted STM images should correspond to a superposition of the two *trans*-configurations and predominantly the left and right *cis*-configurations. Figure 2h shows a schematic diagram of the superposition of the two stable *trans*-configurations as well as the left and right *cis*-configurations at low bias voltage. Clearly, the ratio of the *trans*- versus *cis*-contributions to the image, which depends on the hydrogen-transfer rate, is not relevant in this case. For all ratios, we get a cross-like morphology. However, in Figure 2i, a schematic diagram of the superposition of corresponding states at high bias voltage reveals that the observed image would depend on this ratio. If the hydrogen transfer rate is low, i.e., low probability of the molecule being the *cis*-configuration, we would still observe a cross-like morphology arising from the *trans*-configuration. If the hydrogen-transfer rate is high, however, as we expect at high bias voltages,[7] the *cis*-configurations appear at a frequency that is comparable to those of the two *trans*-configurations and, therefore, make a substantial contribution. The predicted image is as shown in Figure 2i, i.e., a double-C-shaped morphology. Hence, for NPc molecules adsorbed on a Ag(111) surface, a double-C-shaped STM morphology at high bias voltages can be regarded as a new "fingerprint" of the crucial *cis*-configurations in the stepwise hydrogen-transfer process. We emphasize that, if we take into account only the PDOS of the lowest-energy *trans*-state (Figure 2d,f), or even the relative weights of molecular orbitals at low and high bias as well as nonsymmetric binding sites on the surface, we do not obtain the cross-C shape transition at increased bias. The contribution of the *cis*-state PDOS (Figure 2e,g) is essential for the C-shape feature at high bias.

Visualization of Double-C-Shaped Morphologies of NPc/Ag(111) by STM. In order to capture the single-C- or double-C-shaped "fingerprint" of the *cis*-configurations, we deposited NPc molecules on Ag(111). When scanning at RT and a bias of −1.0 V, the STM image of a self-assembled monolayer of NPc molecules on Ag(111) shows a typical cross-like morphology (Figure 3a). The NPc molecules appear as crosses with four clearly resolved outer lobes and a depression in the center.[23] When the bias voltage is increased to −2.5 V, the image of the NPc molecule changes to the symmetric double-C "fingerprint" (Figure 3b). Notably, at high scanning bias, the symmetric double-C morphology of NPc molecules could be observed at RT in all self-assembly monolayer domains on Ag(111) (Supplementary Figure 1), confirming that the thermal ordering of the transfer energy barriers is maintained when high biases induce higher transfer rates. Further experiments reveal that reversible and robust transitions of the STM morphology between cross-like and symmetric-double-C morphologies could be achieved by regulating the scanning bias between −1.0 V and −2.5 V at RT (Figure 3d).

Finally, with a high scanning bias voltage (−2.8 V) at LT (100 K), the STM image shows an *asymmetric* double-C morphology (Figure 3c,e). The high voltage (−2.8 V) causes a high transfer rate, which makes the *cis*-configurations visible. Thus, the asymmetry in the double-C image reflects the fact that, at low temperature, the lowest-energy-barrier path (left path) is dominant, with a smaller contribution from the next-energy-barrier path (right path). This result provides further confirmation that the crucial *cis*-configuration has been visualized. At 100 K, the appearance of asymmetric-double-C in both the full-monolayer coverage where the molecules are ordered (Figure 3c) and the submonolayer coverage where molecules are randomly oriented (Supplementary Figure 6d) suggests that the two double-C morphologies are not caused

https://dx.doi.org/10.1021/acs.jpclett.0c00046
J. Phys. Chem. Lett. 2020, 11, 1536−1541

by differences in the packing of molecules. DFT calculations indicate that the substrate *n*-dopes the NPc molecules but does not induce double-C morphologies by altering the molecule's electronic structure (Supplementary Figure 3).

We have shown that the double-C-shaped structures of NPc molecules at high bias voltage provide a new "fingerprint" for the direct visualization of the metastable *cis*-configurations. Compared with the spectral techniques that have been used to detect the existence of metastable *cis*-configurations,[12−17,26] the STM technique in this paper yields direct high-resolution real-space molecular morphology and can tune the hydrogen-transfer rate by temperature and bias voltage. These merits of the STM technique greatly increase the probability of detecting this crucial metastable configuration during the dynamical transfer process.

In conclusion, a combination of theoretical DFT calculations and experimental STM observations confirm the direct visualization of the crucial metastable *cis*-configuration during the stepwise hydrogen-transfer process of NPc on Ag(111) surfaces. DFT calculations predict that there exists a metastable *cis*-configuration between two stable *trans*-configurations during the hydrogen-transfer process, and the lobes without hydrogen atoms exhibit higher electron density than the lobes with hydrogen atoms, which should result in a single-C morphology in STM at high bias voltage. When the NPc molecules are adsorbed on the Ag(111) surface, it is energetically preferable for the two hydrogens to tunnel through left and right paths. The superposition of both *trans*-configurations as well as the left and right *cis*-configurations leads to a double-C morphology in STM images. Experimentally, using NPc molecules self-assembled on Ag(111) surface as an example, by regulating the scanning bias, we observed the reversible NPc morphology transition between a typical cross morphology and the predicted double-C-shaped morphology. Asymmetric double-C morphology of the NPc molecule has also been visualized for molecules absorbed on Ag(111) at 100 K. The experimental images show excellent agreement with the theoretical simulations. Our findings demonstrate a powerful capability of the STM technique for directly visualizing intermediates in chemical reactions.

■ ASSOCIATED CONTENT

Supporting Information

The Supporting Information is available free of charge at https://pubs.acs.org/doi/10.1021/acs.jpclett.0c00046.

Detailed experimental procedures, calculations methods, figures showing STM images, rate difference and simulations of thermal transfer, *n*-doping effect of the substrate, adsorption configurations, energy profiles, and a tables of percent contributions to transfer rates (PDF)

■ AUTHOR INFORMATION

Corresponding Authors

Qing Huan − *Institute of Physics and University of the Chinese Academy of Sciences, Chinese Academy of Sciences, Beijing 100190, China; CAS Centre for Excellence in Topological Quantum Computation, Chinese Academy of Sciences, Beijing 100190, China*; Email: huanq@iphy.ac.cn

Shixuan Du − *Institute of Physics and University of the Chinese Academy of Sciences, Chinese Academy of Sciences, Beijing 100190, China; CAS Centre for Excellence in Topological Quantum Computation, Chinese Academy of Sciences, Beijing 100190, China; Key Laboratory for Vacuum Physics, Chinese Academy of Sciences, Beijing 100049, China; Songshan Lake Materials Laboratory, Dongguan, Guangdong 523808, China;* orcid.org/0000-0001-9323-1307; Email: sxdu@iphy.ac.cn

Hong-Jun Gao − *Institute of Physics and University of the Chinese Academy of Sciences, Chinese Academy of Sciences, Beijing 100190, China; CAS Centre for Excellence in Topological Quantum Computation, Chinese Academy of Sciences, Beijing 100190, China; Key Laboratory for Vacuum Physics, Chinese Academy of Sciences, Beijing 100049, China;* orcid.org/0000-0002-6766-0623; Email: hjgao@iphy.ac.cn

Authors

Rongting Wu − *Institute of Physics and University of the Chinese Academy of Sciences, Chinese Academy of Sciences, Beijing 100190, China; CAS Centre for Excellence in Topological Quantum Computation, Chinese Academy of Sciences, Beijing 100190, China*

De-Liang Bao − *Institute of Physics and University of the Chinese Academy of Sciences, Chinese Academy of Sciences, Beijing 100190, China; CAS Centre for Excellence in Topological Quantum Computation, Chinese Academy of Sciences, Beijing 100190, China; Department of Physics and Astronomy & Department of Electrical Engineering and Computer Science, Vanderbilt University, Nashville, Tennessee 37235, United States;* orcid.org/0000-0002-5070-4765

Linghao Yan − *Institute of Physics and University of the Chinese Academy of Sciences, Chinese Academy of Sciences, Beijing 100190, China; CAS Centre for Excellence in Topological Quantum Computation, Chinese Academy of Sciences, Beijing 100190, China;* orcid.org/0000-0002-4860-8096

Yeliang Wang − *Institute of Physics and University of the Chinese Academy of Sciences, Chinese Academy of Sciences, Beijing 100190, China; CAS Centre for Excellence in Topological Quantum Computation, Chinese Academy of Sciences, Beijing 100190, China*

Junhai Ren − *Institute of Physics and University of the Chinese Academy of Sciences, Chinese Academy of Sciences, Beijing 100190, China; CAS Centre for Excellence in Topological Quantum Computation, Chinese Academy of Sciences, Beijing 100190, China;* orcid.org/0000-0002-5948-1967

Yan-Fang Zhang − *Institute of Physics and University of the Chinese Academy of Sciences, Chinese Academy of Sciences, Beijing 100190, China; CAS Centre for Excellence in Topological Quantum Computation, Chinese Academy of Sciences, Beijing 100190, China*

Yu-Yang Zhang − *Institute of Physics and University of the Chinese Academy of Sciences, Chinese Academy of Sciences, Beijing 100190, China; CAS Centre for Excellence in Topological Quantum Computation, Chinese Academy of Sciences, Beijing 100190, China; Department of Physics and Astronomy & Department of Electrical Engineering and Computer Science, Vanderbilt University, Nashville, Tennessee 37235, United States; Key Laboratory for Vacuum Physics, Chinese Academy of Sciences, Beijing 100049, China;* orcid.org/0000-0002-9548-0021

Sokrates T. Pantelides − *Department of Physics and Astronomy & Department of Electrical Engineering and Computer Science, Vanderbilt University, Nashville, Tennessee 37235, United States; Institute of Physics and University of the Chinese Academy of Sciences, Chinese Academy of Sciences, Beijing 100190, China;* orcid.org/0000-0002-2963-7545

https://dx.doi.org/10.1021/acs.jpclett.0c00046
J. Phys. Chem. Lett. 2020, 11, 1536−1541

Complete contact information is available at:
https://pubs.acs.org/10.1021/acs.jpclett.0c00046

Author Contributions

[¶]R. Wu and D.-L. Bao contributed equally to this work.

Notes

The authors declare no competing financial interest.

■ ACKNOWLEDGMENTS

This work was financially supported by the National Key Research and Development Projects of China (Nos. 2016YFA0202300, 2018FYA0305800), National Natural Science Foundation of China (Nos. 61888102 and 61725107), Strategic Priority Research Program of the Chinese Academy of Sciences (No. XDB30000000), the CAS Pioneer Hundred Talents Program, Beijing Nova Program (No. Z181100006218023), the International Partnership Program of Chinese Academy of Sciences (Grant number No. 112111KYSB20160061), K. C. Wong Education Foundation, and China Postdoctoral Science Foundation (Grant 2018M641511). Work at Vanderbilt (S.T.P., Y.Y.Z., and D.L.B.) was supported by the U.S. Department of Energy under grant DE-FG02-09ER46554 and by the McMinn Endowment. Computations by Y.Y.Z. and S.T.P. were carried out at the National Energy Research Scientific Computing Center, a DOE Office of Science User Facility supported by the Office of Science of the U.S. Department of Energy under Contract No. DE-AC02-05CH11231. Computations by D.L.B. and Y.F.Z. were carried out at the National Supercomputing Center of Tianjin.

■ REFERENCES

(1) Löwdin, P.-O. Proton tunneling in DNA and its biological implications. *Rev. Mod. Phys.* **1963**, *35* (3), 724.
(2) Tapia, O.; Andres, J.; Safont, V. Theoretical study of transition structures for intramolecular hydrogen transfer in molecular models representing D-ribulose 1,5-bisphosphate. A possible molecular mechanism for the enolization step in rubisco. *J. Phys. Chem.* **1994**, *98* (18), 4821−4830.
(3) Masgrau, L.; Roujeinikova, A.; Johannissen, L. O.; Hothi, P.; Basran, J.; Ranaghan, K. E.; Mulholland, A. J.; Sutcliffe, M. J.; Scrutton, N. S.; Leys, D. Atomic description of an enzyme reaction dominated by proton tunneling. *Science* **2006**, *312* (5771), 237−241.
(4) Stowell, M.; McPhillips, T.; Rees, D.; Soltis, S.; Abresch, E.; Feher, G. Light-induced structural changes in photosynthetic reaction center: implications for mechanism of electron-proton transfer. *Science* **1997**, *276* (5313), 812−816.
(5) Kumagai, T.; Shiotari, A.; Okuyama, H.; Hatta, S.; Aruga, T.; Hamada, I.; Frederiksen, T.; Ueba, H. H-atom relay reactions in real space. *Nat. Mater.* **2012**, *11* (2), 167.
(6) Merte, L. R.; Peng, G.; Bechstein, R.; Rieboldt, F.; Farberow, C. A.; Grabow, L. C.; Kudernatsch, W.; Wendt, S.; Lægsgaard, E.; Mavrikakis, M. Water-mediated proton hopping on an iron oxide surface. *Science* **2012**, *336* (6083), 889−893.
(7) Liljeroth, P.; Repp, J.; Meyer, G. Current-induced hydrogen tautomerization and conductance switching of naphthalocyanine molecules. *Science* **2007**, *317*, 1203−1206.
(8) Auwärter, W.; Écija, D.; Klappenberger, F.; Barth, J. V. Porphyrins at interfaces. *Nat. Chem.* **2015**, *7* (2), 105−120.
(9) Meng, X.; Guo, J.; Peng, J.; Chen, J.; Wang, Z.; Shi, J.-R.; Li, X.-Z.; Wang, E.-G.; Jiang, Y. Direct visualization of concerted proton tunnelling in a water nanocluster. *Nat. Phys.* **2015**, *11* (3), 235.
(10) Maity, D. K.; Bell, R. L.; Truong, T. N. Mechanism and quantum mechanical tunneling effects on inner hydrogen atom transfer in free base porphyrin: a direct ab initio dynamics study. *J. Am. Chem. Soc.* **2000**, *122* (5), 897−906.
(11) Braun, J.; Koecher, M.; Schlabach, M.; Wehrle, B.; Limbach, H.-H.; Vogel, E. NMR study of the tautomerism of porphyrin including the kinetic HH/HD/DD isotope effects in the liquid and the solid state. *J. Am. Chem. Soc.* **1994**, *116* (15), 6593−6604.
(12) Braun, J.; Limbach, H. H.; Williams, P. G.; Morimoto, H.; Wemmer, D. E. Observation of kinetic tritium isotope effects by dynamic NMR. The tautomerism of porphyrin. *J. Am. Chem. Soc.* **1996**, *118* (30), 7231−7232.
(13) Butenhoff, T. J.; Moore, C. B. Hydrogen-atom tunneling in the thermal tautomerism of porphine imbedded in a normal-hexane matrix. *J. Am. Chem. Soc.* **1988**, *110* (25), 8336−8341.
(14) Vdovin, A.; Sepiol, J.; Urbanska, N.; Pietraszkiewicz, M.; Mordzinski, A.; Waluk, J. Evidence for two forms, double hydrogen tunneling, and proximity of excited states in bridge-substituted porphycenes: Supersonic jet studies. *J. Am. Chem. Soc.* **2006**, *128* (8), 2577−2586.
(15) Völker, S.; Van der Waals, J. H. Laser-induced photochemical isomerization of free base porphyrin in an *n*-octane crystal at 4.2 K. *Mol. Phys.* **1976**, *32* (6), 1703−1718.
(16) Butenhoff, T. J.; Chuck, R. S.; Limbach, H. H.; Moore, C. B. Vibrational photochemistry of porphine imbedded in a *n*-Hexane-d_{14} Shpol'skii matrix. *J. Phys. Chem.* **1990**, *94* (20), 7847−7851.
(17) Thomas, K. E.; McCormick, L. J.; Vazquez-Lima, H.; Ghosh, A. Stabilization and structure of the *cis* tautomer of a free-base porphyrin. *Angew. Chem.* **2017**, *129* (34), 10222−10226.
(18) Kumagai, T.; Hanke, F.; Gawinkowski, S.; Sharp, J.; Kotsis, K.; Waluk, J.; Persson, M.; Grill, L. Controlling intramolecular hydrogen transfer in a porphycene molecule with single atoms or molecules located nearby. *Nat. Chem.* **2014**, *6* (1), 41−46.
(19) Ladenthin, J. N.; Frederiksen, T.; Persson, M.; Sharp, J. C.; Gawinkowski, S.; Waluk, J.; Kumagai, T. Force-induced tautomerization in a single molecule. *Nat. Chem.* **2016**, *8* (10), 935−940.
(20) Kumagai, T.; Hanke, F.; Gawinkowski, S.; Sharp, J.; Kotsis, K.; Waluk, J.; Persson, M.; Grill, L. Thermally and vibrationally induced tautomerization of single porphycene molecules on a Cu(110) surface. *Phys. Rev. Lett.* **2013**, *111* (24), 246101.
(21) Koch, M.; Pagan, M.; Persson, M.; Gawinkowski, S.; Waluk, J.; Kumagai, T. Direct observation of double hydrogen transfer via quantum tunneling in a single porphycene molecule on a Ag(110) surface. *J. Am. Chem. Soc.* **2017**, *139* (36), 12681−12687.
(22) Auwärter, W.; Seufert, K.; Bischoff, F.; Ecija, D.; Vijayaraghavan, S.; Joshi, S.; Klappenberger, F.; Samudrala, N.; Barth, J. V. A surface-anchored molecular four-level conductance switch based on single proton transfer. *Nat. Nanotechnol.* **2012**, *7* (1), 41.
(23) Wu, R.; Yan, L.; Zhang, Y.; Ren, J.; Bao, D.; Zhang, H.; Wang, Y.; Du, S.; Huan, Q.; Gao, H.-J. Self-assembled patterns and Young's modulus of single-layer naphthalocyanine molecules on Ag(111). *J. Phys. Chem. C* **2015**, *119* (15), 8208−8212.
(24) Wang, Y. L.; Gao, H.-J.; Guo, H. M.; Wang, S.; Pantelides, S. T. Bonding configurations and collective patterns of Ge atoms adsorbed on Si (111)−(7 × 7). *Phys. Rev. Lett.* **2005**, *94* (10), 106101.
(25) Repp, J.; Meyer, G.; Stojković, S. M.; Gourdon, A.; Joachim, C. Molecules on insulating films: scanning-tunneling microscopy imaging of individual molecular orbitals. *Phys. Rev. Lett.* **2005**, *94* (2), 026803.
(26) Henning, J.; Limbach, H. H. Kinetic study of hydrogen tunnelling in meso-tetraphenylporphine by nuclear magnetic-resonance lineshape analysis and selective $T_{1\rho}$-relaxation time measurements. *J. Chem. Soc., Faraday Trans. 2* **1979**, *75*, 752−766.

Supporting Information

Direct visualization of hydrogen-transfer intermediate states by scanning tunneling microscopy

Rongting Wu[1,†,‡], De-Liang Bao[1,2,‡], Linghao Yan[1], Yeliang Wang[1], Junhai Ren[1], Yan-Fang Zhang[1], Qing Huan[1*], Yu-Yang Zhang[1,2,3], Shixuan Du[1,3,4*], Sokrates T. Pantelides[2,1] & Hong-Jun Gao [1,3*]

[1]Institute of Physics and University of Chinese Academy of Sciences, and CAS Centre for Excellence in Topological Quantum Computation, Chinese Academy of Sciences, Beijing, 100190, China.
[2]Department of Physics and Astronomy & Department of Electrical Engineering and Computer Science, Vanderbilt University, Nashville, Tennessee, 37235, USA
[3]Key Laboratory for Vacuum Physics, Chinese Academy of Sciences, Beijing 100049, China.
[4]Songshan Lake Materials Laboratory, Dongguan, Guangdong 523808, China

[†]Present address: Department of Chemistry, Yale University, New Haven, Connecticut 06511, USA
[‡] R. Wu and D.-L. Bao contributed equally to this work.

*e-mail: sxdu@iphy.ac.cn; huanq@iphy.ac.cn; hjgao@iphy.ac.cn

1. Methods

Experiments: All experiments were carried out in a homemade ultrahigh vacuum (UHV) STM[1] system with the base pressure better than 2×10^{-10} mbar. The single-crystal Ag(111) surfaces were prepared in ultrahigh vacuum by repeated cycles of Ne^+ ion sputtering and subsequent annealing at 770 K until a clean and atomically flat surface was confirmed by STM imaging[2]. 2,3-Naphthalocyanine (NPc, Aldrich, purity >95%) in powder form was purified by a sublimation process with a homemade Knudsen cell (K-cell) evaporator in high vacuum for three days, followed by degassing at 640 K for 2 h in the UHV chamber[3,4]. The NPc was evaporated at 610 K during the experiment, while the substrate Ag(111) was kept at room temperature. For the purposes of this paper, monolayer (ML) is defined as the amount of deposited NPc that entirely covers the substrate surface. All the STM images were taken in constant-current mode, with the bias applied to the sample. The scanning temperature was room temperature (RT) for the monolayer and multilayer structures, but 100 K for sub-monolayer structures, using the continuous cooling method[1].

Calculations: DFT calculations were performed using the VASP code[5,6] with the projector-augmented wave (PAW) method[7]. The Perdew–Burke–Ernzernhof (PBE)[8] version of the generalized gradient approximation (GGA)[9] was used. The plane-wave cutoff was 400 eV. Climbing Image Nudged Elastic Band (CI-NEB) calculations[10,11] were carried out to unveil the nature of the hydrogen transfer process. For an atomic-scale model with an adsorbed NPc molecule, the unit cell contains a three-layer Ag(111) slab and a NPc molecule adsorbed on one side, with lattice parameters a = 16.4 Å and b = 17.9 Å based on the smallest periodic unit of the STM images of a self-assembled NPc monolayer. The vacuum slab is ~22 Å thick. For a freestanding molecule, in the unit cell, the Ag(111) slab was deleted, only leaving the molecule. The vacuum slab was 30 Å thick. The bottom-layer atoms of the Ag(111) slab were fixed, all other Ag atoms and the molecule were fully relaxed until the residual forces were smaller than 0.02 eV/Å in the structural relaxations and 0.05 eV/Å in the CI-NEB calculations, respectively. The Brillouin zone was sampled with only the Γ-point in all calculations. Van der Waals interactions were included using Grimme's[12] empirical correction and the standard value for each element in PBE+D calculations.

2. Double-C shape morphology in all NPc self-assembly domains on Ag(111).

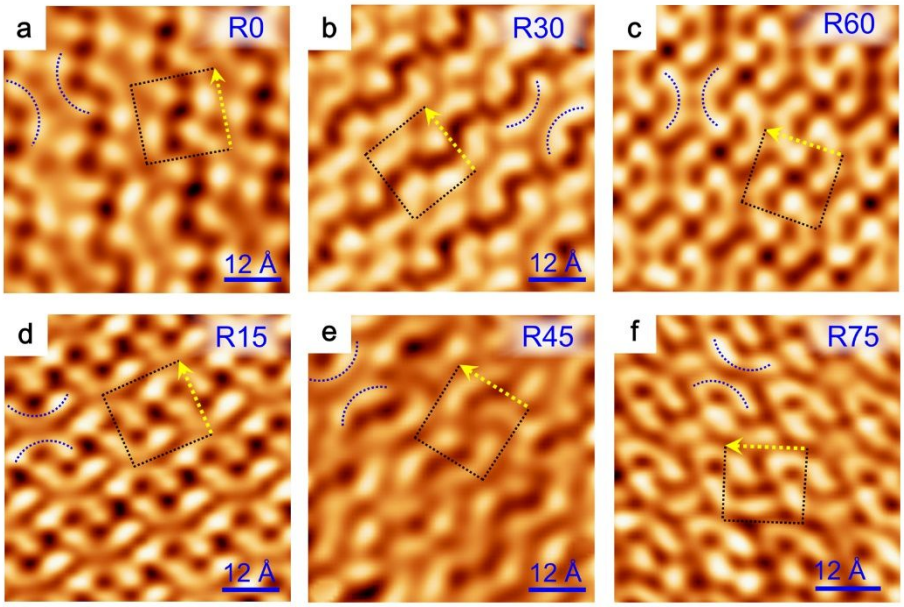

Supplementary Fig. 1 Double-C shape morphology in all of the six NPc molecular self-assembly domains on Ag(111) substrate. The unit cells and crystal orientations of self-assembly molecular domains are highlighted by the dashed rectangles and yellow arrows, respectively. The scanning parameters are: Fig. a, -2.3 V, 0.1 A, Fig. b, -2.75 V, 0.1 nA, Fig. c, -2.3 V, 0.1 nA, Fig. d, -2.3 V, 0.1 nA, Fig. e, -1.5 V, 0.1 nA, Fig. f, -3.3 V, 0.1 nA.

During the experiment, we carried out detailed STM studies on all of the six NPc molecular self-assembly domains. At low scanning bias, all the molecules exhibit a cross-like shape, which was reported in prior work[13]. When the bias is larger than -2.0 eV, all of the NPc molecules in the six self-assembly domains exhibit a double-C-shaped structure, as shown in Supplementary Figure 1. Apparently, all double-C features in each domain exhibit a uniform orientation.

3. Rate difference of thermal-transfer and quantum tunneling for the two-hydrogen transfer process in NPc molecules at fcc site on Ag(111) surface.

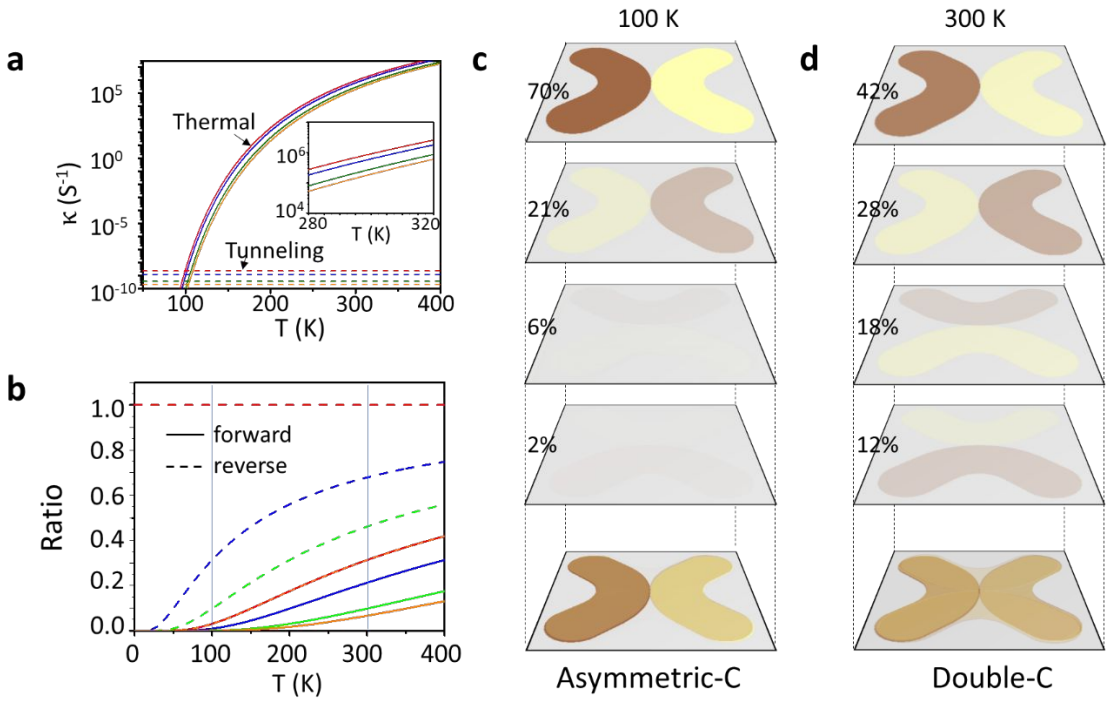

Supplementary Fig. 2 Rate difference and simulations of thermal-transfer and quantum tunneling for the two-hydrogen transfer process in NPc molecules at fcc site on Ag(111) surface. **a,** The plot of the frequencies of the thermal- (solid) and the tunneling-transfer (dashed) as a function of temperature. The four curves in red, blue, green and orange colors correspond to the four paths shown in Fig. 2 in the main text. The inset shows the thermal-transfer results at around room temperature, 300 K. **b**, The plot of the normalized thermal-transfer ratio of the four paths with reference to the path with the lowest barrier. Solid and dashed curves represent transfers *trans-cis-trans'* (forward) and *trans'-cis-trans* (reverse), respectively. **c, d,** Simulation of the composition of the four *cis*-intermediate states at 100 K and 300 K, respectively. The degree of transparency of each figure in **c** and **d** corresponds to the contribution of each *cis*-state.

Both thermal- and tunneling-tunneling hydrogen transfer processes have been studied. From the aspect of thermal-transfer process, the transfer rate is defined as, $\kappa_{\text{thermal}} = \text{A} \times e^{\left(-\frac{E_b - E_0}{k_B T}\right)}$, where A is a pre-exponential factor, E_b is the energy barrier, E_0 is the hydrogen zero-point energy (ZPE), k_B is the Boltzmann constant, and T is the

temperature. The value of A is assumed to be 1.5×10^{13} s^{-1} [14-17]. The hydrogen ZPE, E_0 , is 0.13 eV[18]. The thermal-transfer reaction rates of the four transfer paths as functions of temperature are shown as solid curves in Supplementary Fig. 2a. As shown in the inset, thermal-transfer reaction rates are divided in two groups. The rates of the left and right paths are higher than those of the up and down paths. For the two-hydrogen tunneling effect, the tunneling rate is defined as, $\kappa_{tunneling} = \nu_t P_t$. Here ν_t is the tunneling frequency and is given by $\nu_t = \frac{1}{\pi a}\sqrt{\frac{E_b - E_0}{2m}}$ [17], where a is the width of the barrier and m is the mass of the hydrogen atom. P_t represents the tunneling probability and is given by $P_t = e^{-\frac{2a}{\hbar}\sqrt{2m(E_b - E_0)}}$. Thus, the temperature-independent tunneling rate $\kappa_{tunneling}$ of the four paths can be obtained and shown as dashed lines in Supplementary Fig. 2a. We can see that, at 100 K, the reaction is in a mixed state of thermal-transfer and tunneling effects, while at RT, κ_{thermal} is significantly larger than $\kappa_{tunneling}$, which means that the thermal-transfer effect is dominant at RT for this reaction.

In order to make clear how much the four *cis*-intermediates contribute to the composition morphology in the STM image at RT, we calculated the normalized thermal-transfer ratios, $\kappa_{\Delta} = e^{\left(-\frac{\Delta}{k_B T}\right)}$, of all paths both in the forward and reversed directions, taking the lowest-barrier path as the reference to be a constant 1. Δ represents the difference of the barriers, $\Delta = E_{bi} - E_{bj}$. At low temperature, 100 K, the relative ratios are 0.03, 0.01, 0.001, and 0.00025 for left, right, down and top paths in the forward direction (solid curves in Supplementary Fig. 2b) and 1.0, 0.30, 0.09, and 0.03 for the left, right, down, and top paths in the reversed direction (dashed curves in Supplementary Fig. 2b), respectively. Thus, taking the total transfer probability as 1, the percentages of the four paths are 70%, 21%, 6%, and 2%, respectively. If we set the degree of transparency of each simulation of the *cis*-intermediate according to the probability values, we can obtain an asymmetric-C morphology, as shown in Fig. S2c, which agrees with the STM image at 100 K [Fig. 3(d)] very well. On the other hand, at RT, the relative ratios are 0.31, 0.21, 0.09, and 0.06 in the forward direction and 1.0, 0.30, 0.09, and 0.03 in the reversed direction, respectively. Accordingly, the percentages of the four paths are 42%, 28%, 18%, and 12%, respectively. As shown in the Fig. S2d, the composite schematic shows a symmetric double-C morphology, which

agrees with the STM images at RT in Figs. 3(b). According to the values shown in the TABLE S1, it can be concluded that, at bridge and top sites, the percentages of left and right paths will be even bigger than the other two paths, resulting in more obvious asymmetric-double-C morphologies at 100 K and symmetric-double-C morphologies at 300 K. The values in the Supplementary Table 1 are from the results in Supplementary Fig. 5.

4. The *n*-doping effect of the substrate to the NPc molecules.

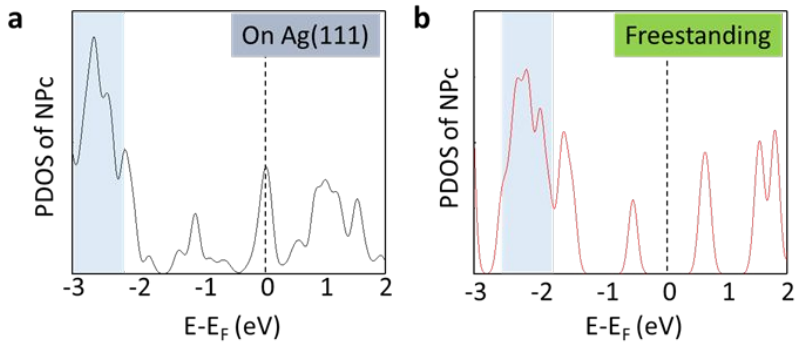

Supplementary Fig. 3 The *n*-doping effect of the substrate on the NPc molecules. **a,** The projected density of states (PDOS) on the NPc molecule (**a**) on Ag(111) surface and (**b**) in the freestanding case. We can see that the states responsible for the double-C image, indicated by blue shading, shift to lower energies in the on-surface case compared to the freestanding molecule. The experimental data, therefore, suggest that the second monolayer is less doped and the third monolayer even less so, as one can reach the imaging DOS window by using progressively smaller voltages. It is not computationally feasible to calculate the PDOS for multilayer-molecule structures to seek confirmation of this inference.

5. Schematic of adsorption sties of NPc molecules on Ag(111) surface.

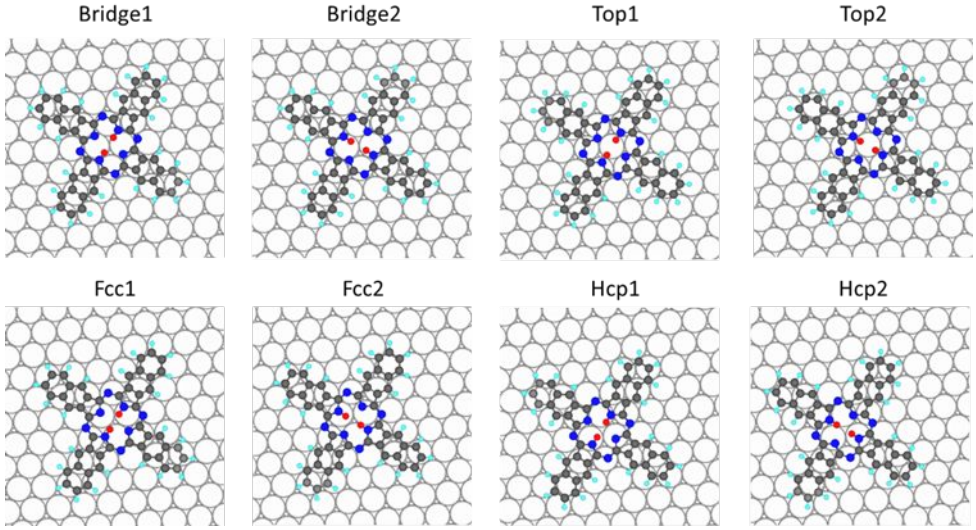

Supplementary Fig. 4 Schematic diagrams of representative adsorption configurations of NPc molecules on a Ag(111) surface**.** Taking the center of the inner cavity as a reference, the molecules are located at bridge, top, fcc, or hcp sites. Numbers 1 and 2 in the site names indicate the initial and final *trans*-isomer arrangements of the H atoms in the molecular cavity.

6. **DFT-calculated energy profiles for the H-transfer paths and schematic of inner cavity of NPc molecules on Ag(111) surface.**

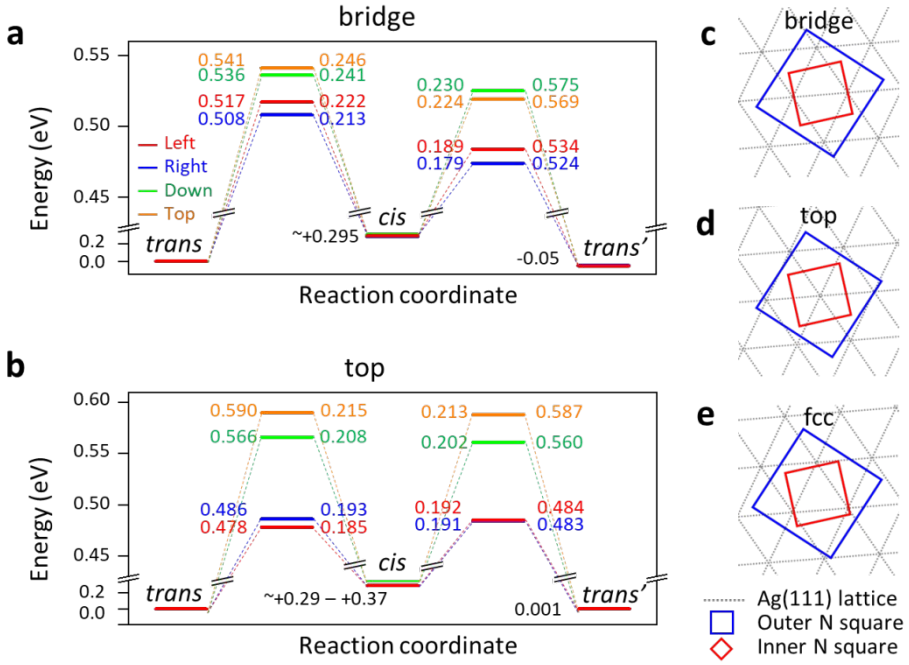

Supplementary Fig. 5 DFT-calculated energy profiles for the H-transfer paths and schematic diagrams of the inner cavity of NPc molecules at different sites on a Ag(111) surface**. a, b,** DFT-calculated energy profiles for the H-transfer paths in NPc molecules at bridge (**a**) and top (**b**) sites. At both sites, the energy barriers of the four H-transfer paths are split in two groups, very much like the case of the fcc site shown in the main text, resulting in double-C STM morphologies. **c-e,** Schematic of the geometric relations between the inner skeletons of NPc molecules and the adsorption-sites of bridge, top, and fcc on Ag(111) surface, respectively. Hcp sites are very similar to fcc sites. It is clear that, the four edges of the inner-N square, which represent the H-transfer trajectories, are different because of the substrate lattice. Despite the different layouts of the substrate at the three types of sites, the four energy barriers split into the same low- and high-energy pairs.

7. **Supplementary Table 1** The percent contributions to the total forward and reverse transfer rates for molecules adsorbed at fcc, bridge and top sites on the Ag(111) surface at 100 K and 300 K.

		left	right	top	down
100 K	**fcc**	70%	21%	6%	2%
	bridge	71%	25%	3%	1%
	top	64%	34%	1%	1%
300 K	**fcc**	42%	28%	18%	12%
	bridge	45%	32%	13%	10%
	top	53%	44%	2%	1%

8. Layer-dependent STM images of the NPc molecules on Ag(111)

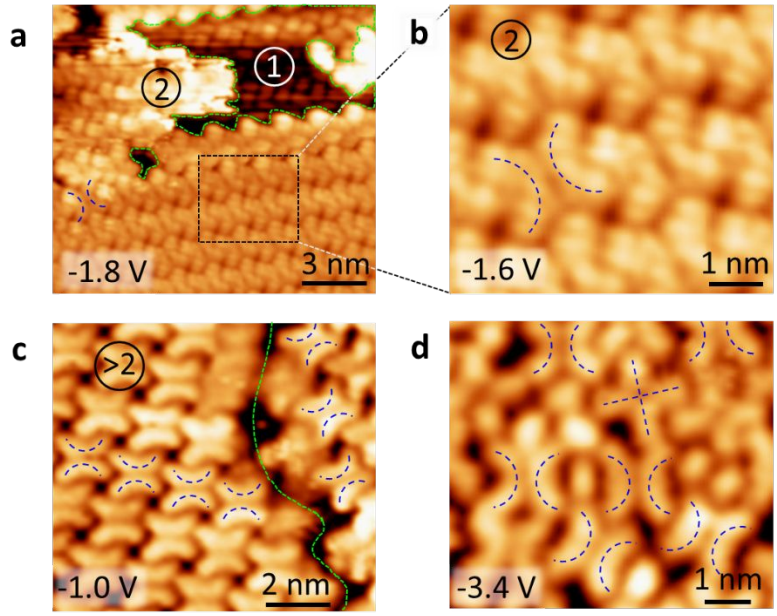

Supplementary Fig. 6 Scanning bias and substrate influence on the STM morphology of NPc molecules. **a**, STM image of the monolayer and bilayer NPc molecules at the bias of -1.8 V. ① represents the first layer and ② represents the second layer. The green dashed curves represent the edge of the top layer. **b**, High-resolution STM image for bilayer NPc molecules within the dashed black square in (**a**), at the bias of -1.6 V. **c**, STM image for multilayer NPc molecules with the bias of -1.0 V. The green dashed line highlights the broad boundary between two domains. **d**, The morphology of sub-monolayer NPc molecules. "Double-C" shapes appear at a quite high bias of -3.4 V. The scanning temperature is 100 K for (**d**) and room temperature for other images.

The "fingerprint" of the *cis*-intermediate, i.e. "double-C" shapes, could also be observed in bilayer and multilayer NPc molecules on Ag(111). To explore the influence of the substrate on the morphological transformation, we fabricated NPc molecular films of different thicknesses on Ag(111), from sub-monolayer to multilayers [Supplementary Fig. 6]. The Supplementary Fig. 6ashows the co-existence of a monolayer (①) and a bilayer (②) of NPc molecules, which exhibit double-C morphologies at a bias of -1.8 V. The high-resolution STM image [Supplementary Fig. 6b] of the second-layer NPc molecules shows double-C morphology and clear electronic states of the molecules at a bias of -1.6 V. The morphology of multilayered NPc molecules is presented in Supplementary Fig. 6c. Scanning at a bias of -1.0 V, the

double-C shaped morphology emerges in both domains. All double-C morphologies are uniform in one domain, but the orientations differ between two domains. Moreover, at 100 K, most of the sub-monolayer NPc molecules present double-C shaped structure at a high bias of -3.4 V, while cross-like molecules could also be observed [Supplementary Fig. 6d]. At sub-monolayer coverage, as shown the Fig. S6(d), the appearance of both double-C and asymmetric-C of the molecules in non-uniform packing indicates that the C-shape morphology is caused by the substrate, not packing. Based on the STM images of NPc molecular films with different thicknesses, it can be concluded that the double-C-shaped image is a ubiquitous feature of the NPc molecules at certain bias voltages.

The top-layer molecules still exhibit a double-C configuration. Since in the crystalline form of NPc molecules the layers are staggered, the symmetry of the top-layer molecules is broken. The ubiquitousness of the double-C morphology in STM images for NPc molecules at distinct sites of the Ag (111) surface and the results of pertinent calculations suggest that the square nature of the NPc molecule leads to two pairs of energy barriers no matter how the symmetry is broken, but it is not practical to perform energy-barrier calculations for such systems to confirm the inference.

References:

(1) Stipe, B. C.; Rezaei, M. A.; Ho, W. A variable-temperature scanning tunneling microscope capable of single-molecule vibrational spectroscopy. *Rev. Sci. Instrum.* **1999,** 70, (1), 137-143.

(2) Wu, R. T.; Ren, J. H.; Dong, L.; Wang, Y. L.; Huan, Q.; Gao, H. J. Quasi-free-standing graphene nano-islands on Ag(110), grown from solid carbon source. *Appl. Phys. Lett.* **2017,** 110, (21).

(3) Yan, L.-H.; Wu, R.-T.; Bao, D.-L.; Ren, J.-H.; Zhang, Y.-F.; Zhang, H.-G.; Huang, L.; Wang, Y.-L.; Du, S.-X.; Huan, Q.; Gao, H.-J. Adsorption behavior of Fe atoms on a naphthalocyanine monolayer on Ag(111) surface. *Chin. Phys. B* **2015,** 24, (7), 076802.

(4) Wu, R.; Yan, L.; Bao, D.-L.; Ren, J.; Du, S.; Wang, Y.; Huan, Q.; Gao, H.-J. Self-Assembly Evolution of Metal-Free Naphthalocyanine Molecules on Ag (111) at the Submonolayer Coverage. *J. Phys. Chem. C* **2019,** 123, (12), 7202-7208.

(5) Vanderbilt, D. Soft self-consistent pseudopotentials in a generalized rigenvalue formalism. *Phys. Rev. B* **1990,** 41, (11), 7892-7895.

(6) Kresse, G.; Furthmüller, J. Efficient iterative schemes for ab initio total-energy calculations using a plane-wave basis set. *Phys. Rev. B* **1996,** 54, (16), 11169-11186.

(7) Kresse, G.; Joubert, D. From ultrasoft pseudopotentials to the projector augmented-wave method. *Phys. Rev. B* **1999,** 59, (3), 1758-1775.

(8) Perdew, J. P.; Burke, K.; Ernzerhof, M. Generalized gradient approximation made simple. *Phys. Rev. Lett.* **1996,** 77, (18), 3865-3868.

(9) Perdew, J. P.; Chevary, J. A.; Vosko, S. H.; Jackson, K. A.; Pederson, M. R.; Singh, D. J.; Fiolhais, C. Atoms, molecules, solids, and surfaces: applications of the generalized gradient approximation for exchange and correlation. *Phys. Rev. B* **1992,** 46, (11), 6671-6687.

(10) Henkelman, G.; Uberuaga, B. P.; Jo´nsson, H. A climbing image nudged elastic band method for finding saddle points and minimum energy paths. *J. Chem. Phys.* **2000,** 113, (22), 9901-9904.

(11) Henkelmana, G.; Jónsson, H. Improved tangent estimate in the nudged elastic band method for finding minimum energy paths and saddle points. *J. Chem. Phys.* **2000,** 113, (22), 9978-9985.

(12) Bučo, T.; Hafner, J.; Lebègue, S.; Ángyán, J. G. Improved description of the structure of molecular and layered crystals: Ab initio DFT calculations with Van der Waals corrections. *J. Phys. Chem. A* **2010,** 114, (43), 11814-11824.

(13) Wu, R.; Yan, L.; Zhang, Y.; Ren, J.; Bao, D.; Zhang, H.; Wang, Y.; Du, S.; Huan, Q.; Gao, H.-J. Self-assembled patterns and Young's modulus of single-layer naphthalocyanine molecules on Ag(111). *J. Phys. Chem. C* **2015,** 119, (15), 8208-8212.

(14) Baetzold, R.; Somorjai, G. A. Preexponential factors in surface reactions. *Journal of Catalysis* **1976,** 45, (1), 94-105.

(15) Cho, J.-H.; Kleinman, L. Dissociative adsorption of vinyl bromide on Si (001): A first-principles study. *Phys. Rev. B* **2005,** 71, (12), 125330.

(16) Guo, H.; Ji, W.; Polanyi, J. C.; Yang, J. Molecular dynamics of localized reaction, experiment and theory: Methyl bromide on Si (111)-7× 7. *ACS Nano* **2008,** 2, (4), 699-706.

(17) Limbach, H.-H.; Miguel Lopez, J.; Kohen, A. Arrhenius curves of hydrogen transfers: tunnel effects, isotope effects and effects of pre-equilibria. *Philosophical Transactions of the Royal Society B: Biological Sciences* **2006,** 361, (1472), 1399-1415.

(18) Gross, A.; Scheffler, M. Role of zero-point effects in catalytic reactions involving hydrogen. *Journal of Vacuum Science & Technology A: Vacuum, Surfaces,*

and Films **1997,** 15, (3), 1624-1629.